THE OFFICIAL MAGAZINE OF THE OCEANOGRAPHY SOCIETY

Oceanography

The Woods Hole Oceanographic Institution surface mooring with ORV *Sagar Nidhi* in the background. *Photo credit: Sean Whelan*

Air-Sea Interaction in the Bay of Bengal

By Robert A. Weller,
J. Thomas Farrar, Jared Buckley,
Simi Mathew, R. Venkatesan,
J. Sree Lekha, Dipanjan Chaudhuri,
N. Suresh Kumar,
and B. Praveen Kumar

ABSTRACT. Recent observations of surface meteorology and exchanges of heat, freshwater, and momentum between the ocean and the atmosphere in the Bay of Bengal are presented. These observations characterize air-sea interaction at 18°N, 89.5°E from December 2014 to January 2016 and also at other locations in the northern Bay of Bengal. Monsoonal variability dominated the records, with winds to the northeast in summer and to the southwest in winter. This variability included a strong annual cycle in the atmospheric forcing of the ocean in the Bay of Bengal, with the winter monsoon marked by sustained ocean heat loss resulting in ocean cooling, and the summer monsoon marked by strong storm events with dark skies and rain that also resulted in ocean cooling. The spring intermonsoon was a period of clear skies and low winds, when strong solar heating and weak wind-driven mixing led to ocean warming. The fall intermonsoon was a transitional period, with some storm events but also with enough clear skies and sunlight that ocean surface temperature rose again. Mooring and shipboard observations are used to examine the ability of model-based surface fluxes to represent air-sea interaction in the Bay of Bengal; the model-based fluxes have significant errors. The surface forcing observed at 18°N is also used together with a one-dimensional ocean model to illustrate the potential for local air-sea interaction to drive upper-ocean variability in the Bay of Bengal.

INTRODUCTION

The atmosphere and the ocean influence each other, and the processes by which this happens are collectively called air-sea interactions. The ocean is heated from above mainly by incoming sunlight, also known as shortwave radiation. As air flows over it, the ocean loses water to the atmosphere by evaporation, and the accompanying ocean cooling is known as latent heat flux. At the same time, the ocean typically loses heat to the atmosphere by sensible heat flux, which includes conduction and convection. Heat and rain from above make the surface of the ocean lighter and more buoyant, building a stable surface layer. Cooling at the surface and salt left behind during evaporation make the surface waters heavier, and the denser water sinks into the interior. Surface water can also be mixed downward by strong winds blowing over the surface, transferring momentum, and driving currents and mixing. On the atmospheric side, air is made more buoyant by release of heat from the ocean and evaporation at the surface that adds water vapor. The ocean provides energy to the atmosphere, drives convection, and supplies moisture to form clouds. Thus, the ocean surface is an important contributor to the dynamics that drive the atmosphere. Many investigators are interested not only in improving understanding of the mechanisms involved in air-sea interaction but also in realistically representing these air-sea interaction processes in models in order to improve predictions of weather and climate features such as the monsoons. In this paper, we refer to the processes that change density as "buoyancy forcing" and to the action of the wind on the water that transfers momentum and drives currents as "wind stress forcing." Buoyancy forcing includes the air-sea exchanges, or fluxes, of heat and of freshwater. Together, buoyancy fluxes and wind stress combine to form the atmospheric forcing that affects or drives the ocean.

Monsoonal variability on a broad spatial scale dominates surface meteorology and air-sea interactions over the northern Indian Ocean, in both the Arabian Sea and the Bay of Bengal. Developing a better understanding of air-sea interactions in the Bay of Bengal has been identified as a key foundation for building an improved capability to predict the monsoons and associated rains that affect so many in southern Asia.

In the Bay of Bengal and the Arabian Sea, strong monsoon winds blow from the southwest to the northeast in summer, and winds that are nearly as strong blow from the northeast to the southwest in winter. In contrast to the Arabian Sea, though, the Bay of Bengal has strong freshwater inputs. Summer and fall rains contribute over a meter of freshwater (Kumar and Prasad, 1997) to the sea surface, and in the northern Bay of Bengal, this freshwater input is augmented by river discharges. The presence of shallow thermohaline structure (temperature and salinity change with depth) and variability of that thermohaline structure associated with the freshwater inputs adds to the complexities of how the upper ocean and lower atmosphere interact. The presence of buoyant freshwater near the surface increases the stability of the surface layer, making it more resistant to being mixed downward, and, at the same time, isolating the deeper ocean from communication with the atmosphere. At times, the water below the surface layer can be warmer than that in the surface layer. Because it is also saltier, the density stratification is stable. However, that warm water is a potential energy reservoir that the ocean can provide to the atmosphere. Thus, there is great interest in understanding when air-sea interactions might expose that warmer water to the atmosphere.

How the ocean and atmosphere in the Bay of Bengal influence each other is not yet fully understood. Various studies have identified either the summer salinity stratification in the Bay of Bengal associated with the freshwater inputs (Shenoi et al., 2002) or the surface buoyancy forcing there (Prasad, 2004) as playing a key role in the processes that control the depth and temperature of the ocean's surface layer, known collectively as mixed-layer dynamics. Thus, much remains to be learned in the Bay of Bengal about how forcing of the ocean surface by the atmosphere contributes to setting the structure and variability of the upper ocean there and about possible feedbacks from the ocean to the atmosphere. In an earlier effort, in 1994–1995, deployment of a well-instrumented surface mooring in the central Arabian Sea captured time series of both the surface forcing and the upper-ocean temperature, salinity, and velocity variability there that provided a foundation for developing a better understanding of the role of air-sea interaction in the central Arabian Sea (Weller et al., 2002). In this paper, we describe very early results from our recent effort to collect similar observations in the Bay of Bengal and begin collaborative research to improve understanding of atmosphere-ocean coupling in the Bay of Bengal.

Observational efforts in the Bay of Bengal include deployment of surface moorings that place meteorological sensors at the sea surface and oceanographic sensors in the upper ocean. We focus here on recent efforts to observe the surface meteorology and air-sea fluxes of heat, freshwater, and momentum in the Bay of Bengal and on using those data to gain insights into how atmospheric variability may govern the structure and variability of the upper ocean there. These are initial contributions to a larger, ongoing effort to better understand the coupled ocean-atmosphere dynamics of the monsoons in the northern Indian Ocean. In this paper, we first summarize our observational methods, which include a surface mooring deployed for 13 months at 18°N, 89.5°E and also the longer-running deployment of surface moorings along 90°E and in the Bay of Bengal. The Research Moored Array for African-Asian-Australian Monsoon Analysis (RAMA) maintained by the National Oceanic and Atmospheric Administration Pacific Marine Environmental Laboratory (NOAA PMEL) and international partners, including India,
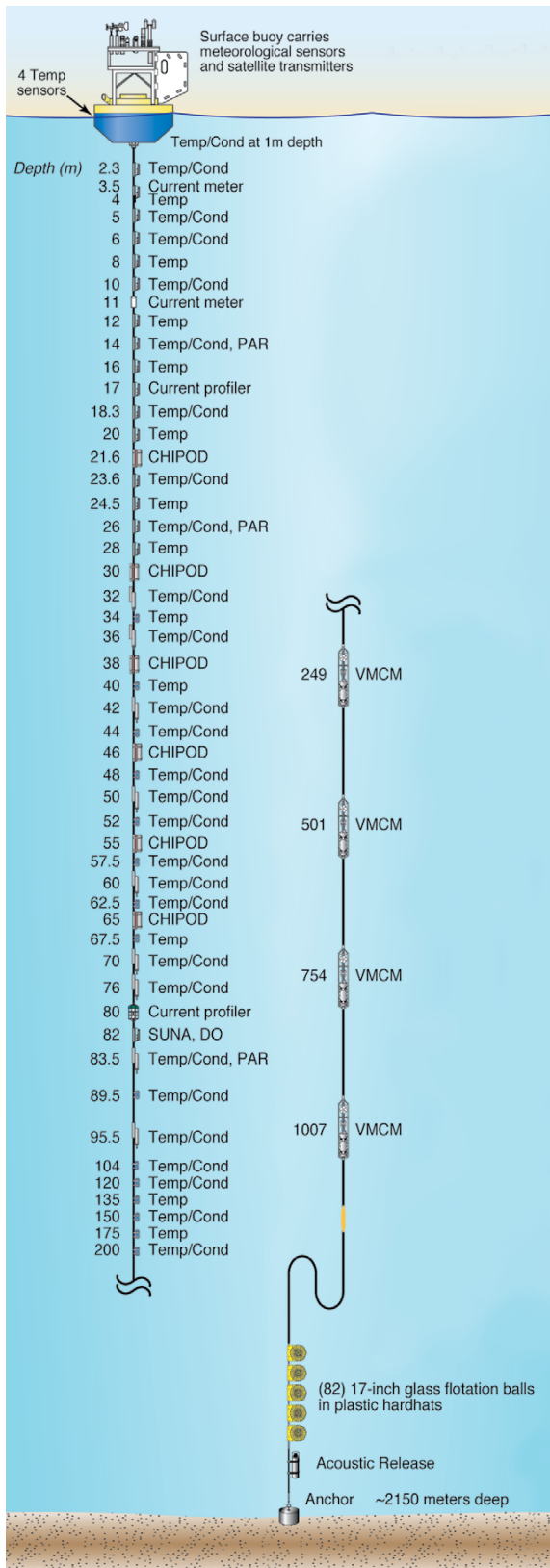
FIGURE 1. (a) Schematic drawing of the Woods Hole Oceanographic Institution (WHOI) surface mooring deployed at 18°N, 89.5°E. The placements are indicated for sensors that measure temperature (Temp), temperature and conductivity (Temp/Cond), turbulence (CHIPOD), velocity (current meter, current profiler, and Vector Measuring Current Meter, or VMCM), dissolved oxygen (DO), photosynthetically available radiation (PAR), and nutrients (SUNA).

includes four different locations along 90°E longitude that have been operational since 2007 (McPhaden et al., 2009). The Ocean Moored Network of buoys for the Northern Indian Ocean (OMNI) is maintained by India's National Institute of Ocean Technology and has been operational since 2011 (Venkatesan et al., 2013). We examine data from the RAMA mooring at 15°N, 90°E and from the OMNI mooring at 18°N to understand the interannual variability of air-sea fluxes. We present a time series of surface meteorology and air-sea fluxes from these select sites. These data allow us then to compare in situ time series with model-based time series of surface meteorology and air-sea fluxes and thus comment on the challenges associated with using these model-based fields. Finally, we use the 13-month time series of surface forcing at 18°N, 89.5°E to drive a one-dimensional ocean model and examine the potential for local atmospheric forcing to drive upper ocean variability in the Bay of Bengal. We end the paper with a summary and conclusions.

OBSERVATIONAL METHODS

The need for observations of the surface meteorology and air-sea fluxes of heat, freshwater, and momentum in the Bay of Bengal was addressed by deployment of surface moorings that have meteorological sensors on the surface buoy and at the same time oceanographic sensors attached to the line that is connected to an anchor on the seafloor (Figure 1). The surface buoy carries batteries, data loggers, and hardware to send some data back via satellite. Averaged meteorological data are telemetered, and the raw data, with a higher sampling rate, are recorded onboard the buoy. Most often, the oceanographic instruments on the mooring line record their data internally; telemetering of subsurface ocean data adds cost but is becoming more common. At the end of the deployment, the mooring releases its connection to the anchor and is recovered. Among the challenges faced during the deployment are damage from fishing gear deployed at or near the mooring and growth of marine organisms on the sensors.

As part of the recent joint Air-Sea Interactions Regional Initiative (ASIRI) and Ocean Mixing and Monsoon (OMM) program, one such surface mooring was deployed at 18°N, 89.5°E from December 2014 to January 2016 by investigators from Woods Hole Oceanographic Institution (WHOI). At the same time, RAMA surface moorings were in place in the Bay of Bengal along 90°E as part of that ongoing effort to observe and monitor the tropical Indian Ocean. Indian development of sustained observing in the Bay of Bengal had also led to ongoing observing at a Bay of Bengal Observatory and several mooring sites. The northern bay exhibits significant variability in salinity and sea surface temperature with considerable influx of freshwater from rivers and shows large intraseasonal oscillation signals during the southwest monsoon season (Vinayachandran et al., 2002; Sengupta et al., 2006). We thus confined our analysis to the moorings located at and to the north of 15°N, one at 15°N, the northernmost RAMA mooring along 90°E longitude, the 17.85°N, 89.67°E OMNI mooring, and the 18°N, 89.5°E WHOI mooring. Figure 2 shows the location of the ASIRI-OMM surface mooring, labeled WHOI, the RAMA mooring, and the Indian OMNI surface mooring (BD09) whose data are discussed in this

paper. We use daily averages when plotting RAMA and OMNI data.

The WHOI surface mooring deployed at 18°N, 89.5°E had a 3 m diameter surface buoy with a tower for meteorological sensors and a bridle below the buoy for attaching the mooring line. Two ASIMET (Air-Sea Interaction Meteorology) systems (Hosom et al., 1995) were installed, each with sensors for wind speed and direction, air temperature and humidity, sea temperature and salinity, incoming shortwave and longwave radiation, barometric pressure, and precipitation. Meteorological sensors are located approximately 3 m above the sea surface, and the ocean salinity and temperature sensors are located on the buoy bridle at 1 m depth. These sensors provided one-minute averages that were recorded, and the ASIMET systems also provided one-hour averages that were telemetered via satellite during the deployment. A third meteorological instrument, a Vaisala WXT 520 that sampled wind speed and direction, barometric pressure, precipitation, and air temperature and humidity, was deployed for further redundancy. The multiple records, together with laboratory calibrations, determined the accuracies of the buoy observations in the field, which are described in Colbo and Weller (2009).

The WHOI mooring was deployed from ORV *Sagar Nidhi* on December 8, 2014, and recovered by ORV *Sagar Kanya* on January 29, 2016. At this point, we have carried out preliminary quality control and evaluation of the surface meteorological data. Both ASIMET systems provided complete records, as did the Vaisala WXT 520. The one-minute surface meteorological data were used to make one-hour surface meteorological time series. These data, in turn, were used with equations known as the bulk formulae to compute hourly time series of the surface fluxes of heat, freshwater, and momentum; Weller et al. (2012) describe the buoy sensors and calculation of the air-sea fluxes in detail, and Bigorre et al. (2013) discuss the accuracies of the buoy meteorology and

fluxes. The heat flux between the ocean and the atmosphere, with a positive sign associated with heating of the ocean, is the sum of net shortwave radiation (solar insolation), net longwave radiation (infrared radiation), latent heat flux (the cooling during evaporation), and sensible heat (direct transfer by conduction and convection). Freshwater flux is the difference between precipitation and evaporation. Momentum flux is a measure of the horizontal momentum transferred between the atmosphere and the ocean, comprised dominantly of the action of the wind on the water that propels wind-driven currents. The heat and freshwater flux are sometimes referred to together as the buoyancy flux. Both heat and the addition of freshwater, which is less dense than seawater, are buoyancy fluxes that make the surface ocean less dense and thus more stable. Both cooling and evaporation (which leaves salt behind) make the surface ocean denser and can cause surface water to sink. Strong winds that drive strong surface currents can also cause mixing of surface waters with those below.

The bulk formulae known as version 3.0 of the Tropical Ocean Global Atmosphere Coupled Ocean Atmosphere Response Experiment (TOGA COARE) flux algorithm (Fairall et al., 2003) were used to calculate wind stress, latent heat flux, and sensible heat flux. A prescribed albedo (reflection from the sea surface) was used together with incoming shortwave radiation to determine net shortwave radiation entering the ocean, and a modified blackbody radiation formula

was used to estimate longwave radiation leaving the sea surface so that with measured incoming longwave radiation the net longwave radiation was computed. In our discussion to follow, positive heat flux is associated with the ocean gaining heat and negative heat flux with the ocean losing heat to the atmosphere.

The WHOI mooring line included oceanographic instruments that measure only temperature, that measure both temperature and the electrical conductivity of the seawater, and that measure horizontal water velocity. By measuring both ocean temperature and conductivity, salinity can be computed. Together, ocean temperature and salinity at a known depth and pressure allow us to compute seawater density. Ocean currents or horizontal velocities were measured at a number of depths (Figure 1). Some instruments measured sound velocity only at the instrument depth. Others instruments had upward-looking sonars and could obtain velocities at many different discrete distances away from their sensors. These latter instruments are known as current profilers, as they yield a vertical profile of ocean currents over the depth range they sample. Several specialized instruments were also deployed. χpods (labeled CHIPOD in the figure) measured rapid fluctuations in temperature in order to sample turbulent mixing. One dissolved oxygen sensor was deployed. At several depths, sensors were deployed to measure the photosynthetically available radiation (PAR). One sensor (SUNA) was deployed to measure the nutrient
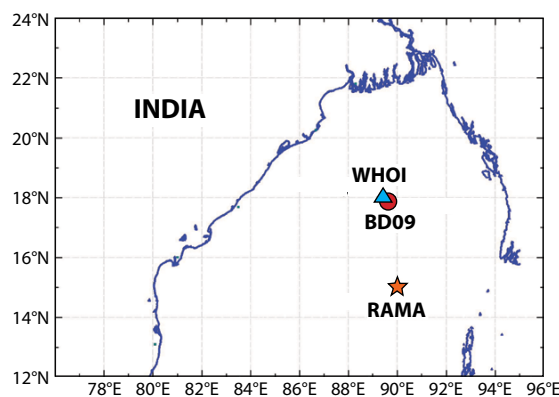

FIGURE 2. Map of the Bay of Bengal showing the locations of the surface moorings discussed in this paper. WHOI mooring = triangle at 18°N, 89.5°E. Ocean Moored Network of buoys for the Northern Indian Ocean (OMNI) mooring BD09 = circle at 17.85°N, 89.67°E. Research Moored Array for African-Asian-Australian Monsoon Analysis (RAMA) mooring = star at 15°N, 90°E.

nitrate. The oceanographic instrumentation was concentrated in the upper 200 m of the water column, where the presence of freshwater was anticipated, where the impact of the surface forcing could be observed, and where we were most intent on learning about the processes at work there that could change the properties (temperature and salinity) and the structure of the upper ocean.

The RAMA mooring at 15°N, 90°E provided high temporal resolution sampling of surface meteorological data along with surface to subsurface measurements of temperature, salinity, and currents (McPhaden et al., 2009). This mooring, which has been operational since 2007, also measured downward longwave radiation, which is required for computation of heat flux. The Indian mooring referred to as the OMNI buoy, which has been operational in the Bay of Bengal since 2011, samples surface meteorology as well as surface and subsurface temperature, salinity, and currents at one-hour intervals. All surface meteorological sensors were fitted on a mast at a height of 3 m, and temperature and salinity were measured at the surface using a Sea-Bird conductivity-temperature instrument that was attached to bottom of the buoy hull. Surface currents were

measured using a downward-looking Doppler Volume Sampler (DVS) that was mounted at the bottom of the hull. The downward-looking acoustic Doppler current profiler (ADCP) attached to the mooring at 7 m depth measured currents with a vertical resolution of 5 m from 10 m to 105 m depth. The accuracies, resolution, and range of all sensors meet the standards recommended by World Meteorological Organization and are listed in Venkatsen et al. (2013).

SURFACE METEOROLOGY AND AIR-SEA FLUXES
At the WHOI Mooring at 18°N During ASIRI in 2015

Monsoonal variability was evident in the data, with strong winds to the northeast during the summer monsoon. Figure 3 provides an overview by showing a time series of the monthly means. One-minute vector-averages of wind velocity had peak speed values that approached 20 m s⁻¹, and hourly averages in the summer monsoon had a maximum of 13.5 m s⁻¹. Winter monsoon winds were not as strong; the hourly maximum was 11.2 m s⁻¹. The winter monsoon winds, coming off the continent, brought the driest and coolest air of the year. Six percent of the annual rain and some cloud cover

events accompanied the winter monsoon; more often, the days were clear and accompanied by midday insolation of up to 700–800 W m⁻². As the winter monsoon ended, a period of very low wind speeds marked the spring intermonsoon in February to April. This was accompanied by the most cloud-free skies and strongest insolation of the year, with only about 3% of the annual rain. The summer monsoon, with 65% of the annual rain at the buoy (close to 2 m), was characterized by moist air and cloud cover. On some days, cloud cover reduced midday insolation to under 100 W m⁻², and this dense cloud cover persisted for several days at a time. The monthly averaged incoming shortwave radiation in July was the lowest of the whole year and was accompanied by the highest monthly rain rate of over 0.8 mm hr⁻¹; the monthly total for July was over 0.62 m. Although the air was moist during the summer monsoon, air and sea surface temperatures both decreased slightly. The fall intermonsoon was a transitional period, with less overall cloud cover, but it was also marked by the occurrence of a number of rainy, cloudy wind events and 26% of the annual rain. Sea surface temperature and air temperature warmed through October, humidity decreased, and insolation recovered from the summer minimum but was lower than during the spring intermonsoon. With the exception of the summer monsoon, midday incoming solar radiation maxima were often observed close to local noon.

The one-year record of monthly averaged air-sea fluxes reflects this annual march of the monsoon climate and the characteristic shorter time scale variability within each season (Figure 4). Wind stress forcing dominated the summer monsoon; the weakest wind stress forcing was observed in the spring intermonsoon. The winter monsoon was a time of sustained net heat loss, with the largest latent heat losses of the year accompanying the drier air of that season. The drier and cooler atmosphere and reduced cloud cover during the winter monsoon also led to the largest net longwave losses of
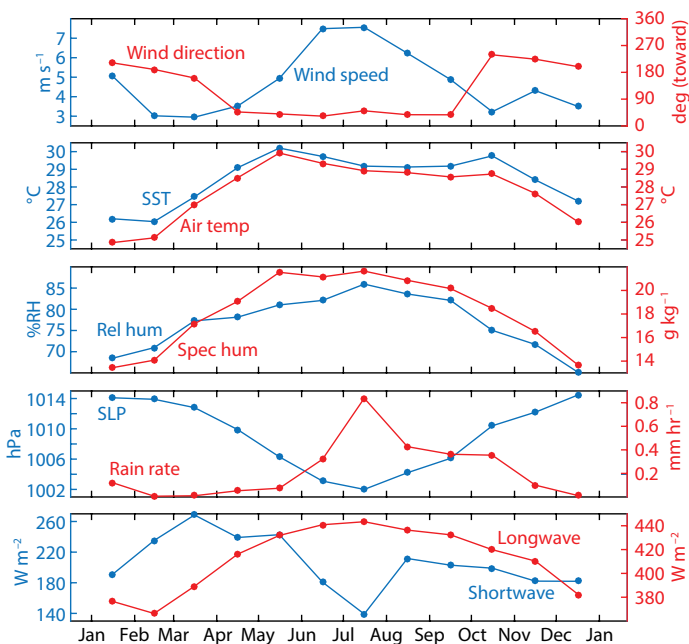

FIGURE 3. Monthly averaged meteorological observations from the WHOI surface mooring. From top to bottom: wind speed and wind direction (toward), air temperature and sea surface temperature, relative and specific humidity, sea level pressure and rain rate, and incoming shortwave and longwave radiation.

the year. However, due to the clear skies, insolation was moderately strong and hourly net heat flux during the winter monsoon typically showed strong positive values through midday when insolation exceeded the heat loss from latent, sensible, and net longwave heat flux. Clear skies persisted during the spring intermonsoon, with the highest monthly net shortwave values of the year and reduced latent and sensible heat losses. These conditions led to the highest net heat flux values and sustained, strong ocean heating and strong midday heating as seen in hourly time series of heat fluxes. That strong diurnal heating by the sun was often coincident with low wind forcing.

With the onset of the summer monsoon, cloud cover reduced the net shortwave heat flux, and the lowest value of monthly mean solar heating was recorded in July. During the summer monsoon, for days at a time during a wind event, the net heat flux remained negative, without enough sunlight to return it to a positive value even at midday. Reduced solar heating was the key contributor to sustained ocean cooling events, as the latent and net longwave heat losses were reduced during the summer monsoon relative to the spring intermonsoon due to the higher humidity of the air and cloud cover. During the fall intermonsoon, fewer very cloudy periods occurred, and solar heating was sufficient to bring monthly net heat air-sea flux to values near +50 W m^{-2}.

Across the Northern Bay of Bengal and During Other Years

The shortwave radiation at the other Bay of Bengal locations showed the same large seasonal variability, with peaks during the spring intermonsoon transition months and lower values during the winter monsoon. In addition, there were large reductions in shortwave radiation during the summer monsoon season owing to cloud coverage (Figure 5a). Net shortwave radiation time series observed from the RAMA mooring at 15°N showed the impact of large cloudy, convective systems
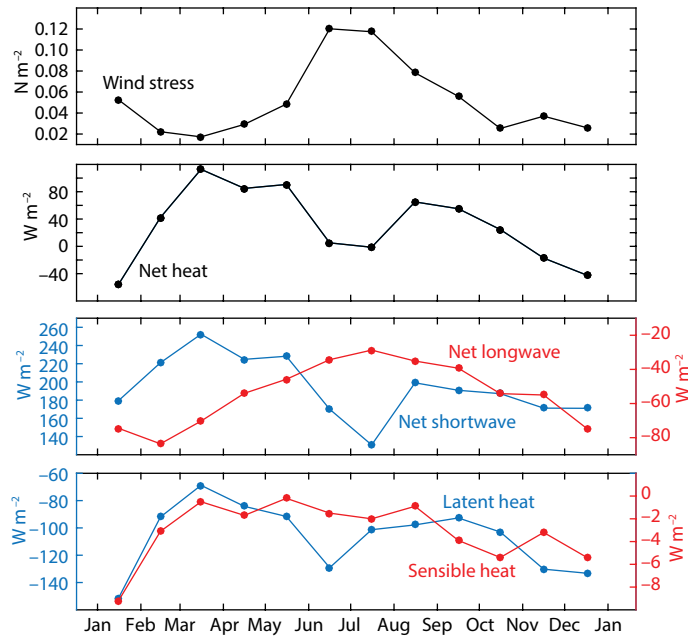

FIGURE 4. Monthly averaged wind stress and heat fluxes from the WHOI surface mooring. From top to bottom: magnitude of wind stress, neat air-sea heat flux, net shortwave and net longwave radiation, and latent and sensible heat flux.
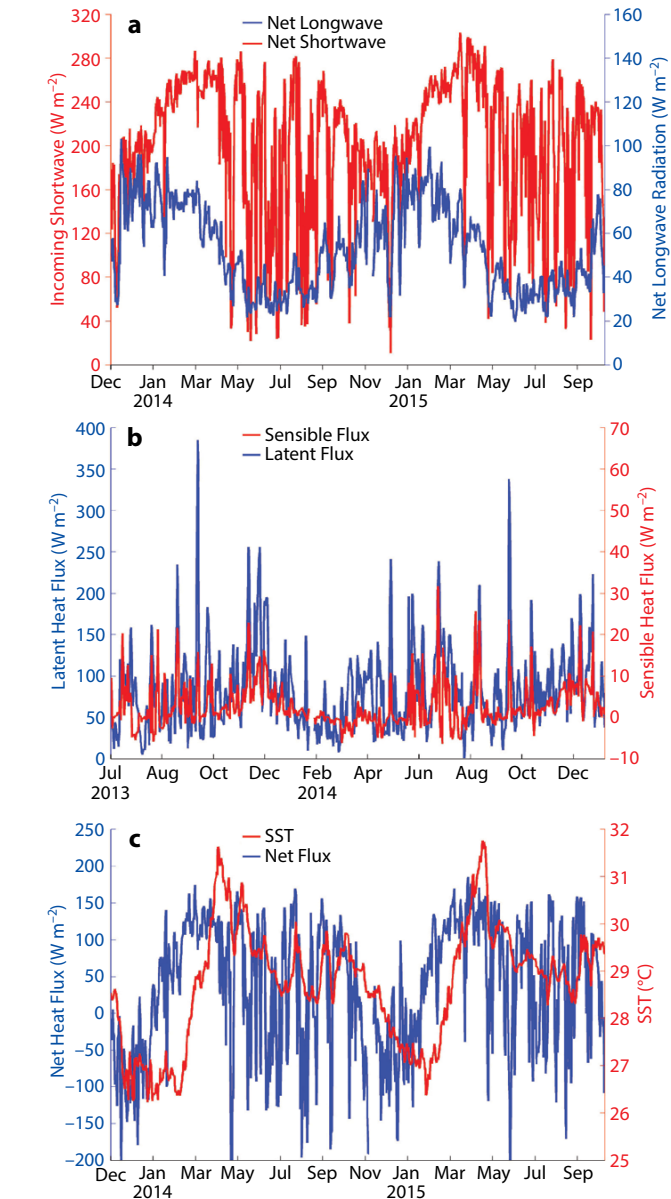

FIGURE 5. (a) Annual variation of net longwave (blue) and net shortwave radiation (red) near the RAMA mooring at 15°N, 90°E. Net longwave is plotted as a positive value to allow overplotting. (b) Latent heat flux (blue) and sensible heat flux (red) time series computed from the OMNI mooring at 18°N, from July 2013 to January 2015, plotted as positive values. (c) Sea surface temperature (red) and net heat flux (blue) during the southwest monsoon season of 2014 as observed by the RAMA mooring at 15°N, 90°E, plotted as daily averages.

formed in the atmosphere over northern Bay of Bengal during summer monsoon season that at times reduced the incoming shortwave radiation by nearly 240 W m^{-2}. An opposite annual cycle was observed in net longwave radiation, which peaked during the winter monsoon and reached a minimum during the summer monsoon months of June to September at the same mooring. The large variability in incoming shortwave radiation during the summer monsoon is due to significant cloud coverage. Rainfall data obtained from the buoy supports this conclusion, with large amounts of rainfall recorded during the summer monsoon as compared to all other seasons. The other two major components of net heat flux are latent heat flux and sensible heat flux. They also showed a seasonal cycle, with the largest latent heat flux during the winter monsoon period,

associated with strong winds and dry air driven into the northern bay by northeast winds (Figure 5b). Secondary peaks in latent heat flux were observed in conjunction with ocean warming events lasting roughly 25 to 90 days over the northern bay during the summer monsoon (thought to be associated with atmospheric variability on those time scales, known as intraseasonal oscillations, or ISOs) and with cyclonic events during the winter transition months, as captured by the OMNI mooring at 17.85°N, 89.67°E (known as BD09; Figure 5b). The sensible heat flux, though a relatively small contributor in the mean to net heat flux, did show peaks exceeding 20 W m^{-2} during episodes within the monsoon season (Figure 5b). Earlier observations by Bhat (2002) noted episodic increases in air-sea temperature difference, accompanied by

higher wind speeds that led to increased sensible heat flux in the northern Bay of Bengal.

COMPARISON OF IN SITU AND MODEL-BASED SURFACE METEOROLOGY AND AIR-SEA FLUXES

Atmospheric reanalysis models provide an alternate source of air-sea fluxes when in situ data are unavailable. Other studies have evaluated atmospheric reanalysis air-sea flux errors globally using in situ data (Brunke et al., 2011; Decker et al., 2012). We compared in situ data from four research cruises in the Bay of Bengal and from the WHOI mooring to the air-sea fluxes of four atmospheric reanalysis models (Figure 6). The four cruises took place aboard R/V *Revelle* as part of the ASIRI experiment (Lucas et al., 2014; Wijesekera et al., in press). The four atmospheric reanalysis models used in the comparison were: National Centers for Environmental Prediction (NCEP) reanalysis 1 (Kalnay et al., 1996), European Centre for Medium-Range Weather Forecast (ECMWF) ERA-Interim (European Centre for Medium-Range Weather Forecasts, 2012), National Aeronautics and Space Administration Modern-Era Retrospective Analysis for Research and Applications (NASA MERRA 1; Global Modeling and Assimilation Office, 2008), and NASA MERRA 2 (Global Modeling and Assimilation Office, 2015).

The in situ and MERRA 1 and 2 data were averaged to six-hourly values for comparison with the six-hourly values from the ECMWF and NCEP reanalysis models. There were 1,760 six-hourly in situ data points available. The nearest grid points in the reanalysis models to the location of the in situ data were used in the comparison.

Table 1 shows the mean air-sea flux values from the four reanalysis models, and Figure 6 compares the time series of net heat flux at the WHOI surface mooring. There is a significant spread in the net heat flux between the models and the
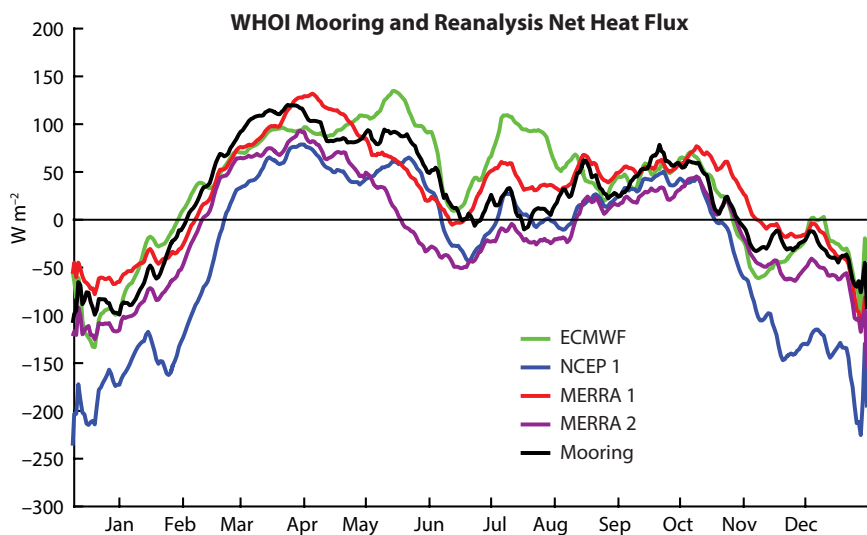

FIGURE 6. Comparison of model net air-sea heat flux from the nearest grid point with net heat flux from the WHOI surface mooring.

TABLE 1. Mean flux values for in situ and reanalysis models.

	Shortwave (W m^{-2})	Longwave (W m^{-2})	Latent (W m^{-2})	Sensible (W m^{-2})	Net (W m^{-2})	Wind Stress (N m^{-2})
In situ	188.9	−53.4	−112.8	−3.9	18.7	0.0614
ECMWF	203.3	−57.4	−113.0	−6.4	26.4	0.0520
NCEP 1	197.7	−60.6	−153.6	−12.8	−29.3	0.0524
MERRA 1	201.6	−66.0	−106.2	−4.3	25.1	0.0512
MERRA 2	187.6	−63.4	−131.9	−6.2	−14.0	0.0673

ECMWF = European Centre for Medium Range Weather Forecasts
NCEP = National Centers for Environmental Prediction
MERRA = Modern-Era Retrospective Analysis for Research and Application

mooring throughout the year (Figure 6). The spread is particularly large during the summer and winter months, with better agreement between the mooring and reanalysis models in spring and fall. The summer spread increase is attributed to overestimation of net heat gain shown in ECMWF and the extended period of net heat loss shown in MERRA 2, while the winter spread increase is attributed to the significant overestimation of net heat loss shown in NCEP 1. Mean net heat flux values vary considerably between the reanalysis models. None of the reanalysis models were particularly skillful in producing realistic net heat flux, although fortuitous cancellation of errors in the various heat flux components brings ECMWF ERA-Interim and MERRA 1 to within 10 W m^{-2} of the in situ observations of net heat flux. All of the reanalysis models overestimated net shortwave radiation except MERRA 2. All of the reanalysis models overestimated net longwave radiation heat loss. Wind stress was better predicted by the models, with MERRA 2 closest to in situ observations. Overestimation of solar heating during the day and surface cooling at night often resulted in a stronger diurnal cycle than seen in the observations. Comparisons with cruise data showed larger reanalysis air-sea flux errors on shorter time scales (<4 weeks).

THE CONTRIBUTION OF LOCAL FORCING TO UPPER OCEAN VARIABILITY

The Price-Weller-Pinkel (PWP) one-dimensional ocean model (Price et al., 1986) was run with the hourly time series of surface fluxes observed at the WHOI mooring (18°N, 89.5°E), and with the temperature and salinity profiles initialized using a conductivity-temperature-depth (CTD) profile obtained near the mooring in January 2015. Figure 7 shows the hourly magnitude of the wind stress and the low-passed (three-day running mean) net heat flux from the WHOI mooring, the observed and modeled hourly SST, and the hourly model mixed layer

depth based on where the density gradient exceeded -2×10^{-4} kg m^{-3} per meter, an overplot of low-passed (25-hour running mean) model and observed mixed layer depths, and an overplot of hourly model and observed surface salinities. To account for the fact that sunlight penetrates the sea surface and that some of the solar heating is thus absorbed below the surface, the PWP model uses the double exponential formulation for optical extinction after Paulson and Simpson (1977); a red light absorption depth of 0.4 m and a blue-green light absorption depth of 20 m were used.

Surface forcing in late fall and winter was characterized by clear skies and resultant positive surface heating during midday alternating with cooling during

the night in response to the combination of latent, sensible, and net longwave heat loss. The model SST shows net SST cooling through this period and, at the same time, an ocean surface mixed layer that shoals around local noon on most days in response to solar heating. This leads to the rapid daily up and down of the model mixed layer depth shown in Figure 7. At the same time, because of significant nighttime cooling, the nighttime mixed layer penetrates deeply, and mean or low-passed mixed layer depths during the winter monsoon are close to 50 m in the model. The spring intermonsoon, with low winds and clear skies, was marked in the model simulation by a shallow mixed layer and a number of diurnal warming and restratification events. Midday spikes
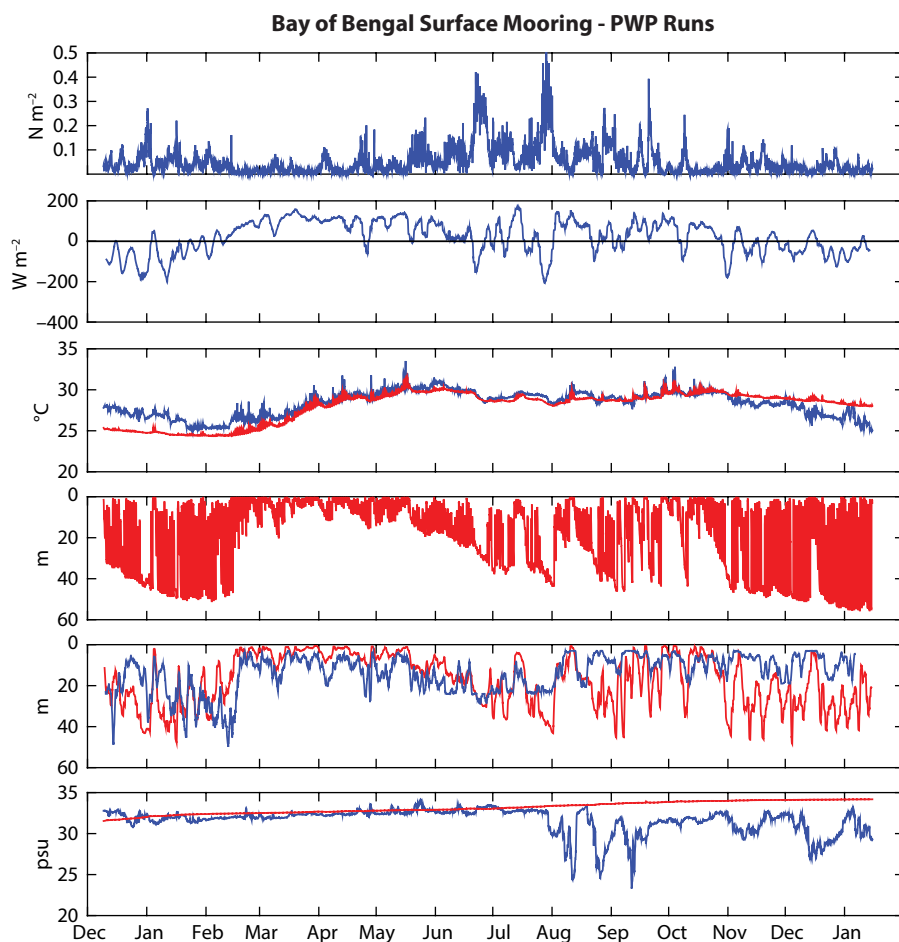

FIGURE 7. Time series of the magnitude of the wind stress from December 2015 to January 2016 (top), low-passed net heat flux (three-day running mean), overplot of observed SST (blue) and model SST (red), hourly model mixed layer depth, overplot of 25-hour running mean of observed and model mixed layer depth, and overplot of hourly observed (blue) and model (red) surface salinity (bottom).

in model SST were seen and on many days replicated the midday diurnal warming spikes observed in SST by the sensors on the buoy. During the summer monsoon, rain and wind events were accompanied by cloud cover that persisted for several days, lowering solar heating and leading to net cooling and periods of several days without any ocean warming. In response, the model SST showed periods of cooling and mixed layer deepening. The storm events led to accompanying periods of a relatively deep ocean mixed layer without diurnal restratification. Less cloud cover and less wind forcing in the fall intermonsoon led to SST warming again and several periods of diurnal restratification and of shallow ocean mixed layers in the model.

This model run, initialized with a January CTD profile, included the freshwater input from local rainfall, but could not and did not include freshening of the upper ocean in the summer and fall resulting from advection of river inputs. The initial difference between the observed and model mixed layer depths beginning in July and persisting to December and January is believed to reflect the lack of freshwater in the model that is evident in the mooring data in the surface salinity time series. The drift of model SST away from observed SST beginning in November and lasting through December and January is also thought to stem from the inability of the one-dimensional model to replicate the influence of the freshwater riverine input. This is reinforced by the low-passed model mixed layer depth often being much deeper than the observed mixed layer depth from late July 2015 onward and, at the same time, by the model sea surface salinity slowly becoming more saline while the observed sea surface salinity shows dramatic freshening events and stays fresher for the remainder of the year. There are additional ocean processes that the model cannot reproduce. The current meter data from the WHOI mooring showed that a strong eddy moved through in July to August 2015. The advective influences

and change in vertical structure due to this eddy and also due to frontal structures cannot be replicated by the model.

SUMMARY AND CONCLUSIONS

Using the observations collected from the ASIRI-OMM and RAMA mooring deployments, we developed a good understanding of the annual march of the surface forcing of the ocean by the atmosphere. Winter monsoons with drier air out of the northeast, little rain, and moderate cloud cover led to sustained ocean cooling. Mean SSTs and air temperature are then the coolest of the year, but midday positive buoyancy flux can drive warming of the ocean and formation of a shallow warm layer midday. During the spring intermonsoon, the positive buoyancy flux is even stronger, and with low winds, frequent diurnal warming of the ocean should be expected together with shallow ocean surface mixed layers. During the summer monsoon, very thick cloud cover does more than offset the astronomical increase in sunlight reaching the Northern Hemisphere in summer, and periods of dark days are marked by sustained negative buoyancy forcing together with strong wind stress forcing, driving ocean cooling, with persisting deeper ocean surface layers anticipated. The fall intermonsoon is marked by higher positive buoyancy forcing and less-frequent wind events, with SST and air temperature recovering before the winter monsoon.

Variability on a number of time scales is embedded in the annual march of the monsoons. The diurnal cycle of insolation and a midday return to positive buoyancy forcing of the ocean surface is often evident. There are the strong forcing events, most often seen in the summer monsoon, where heavy rain and dark clouds persist; these lead to negative buoyancy forcing that persists for three to seven days at a time. In addition, there is evidence in the spring and summer of oscillations in SST at ISO time scales, which suggests a coupling between atmosphere and ocean on those scales. However, we learned from

comparing observed fluxes with model-based fluxes that caution should be used when using model-based fluxes in studies, as the model-based fluxes can be in error. Still, our work so far with the one-dimensional PWP model has been instructive, as the model replicates much of the year's SST time series, including diurnal warming events, variability in spring and summer associated with ISO time scales, and strong summer monsoon storm events. We look forward to processing, and beginning to work with, more of the oceanographic data recovered from the moorings and proceeding further to better understand air-sea interaction in the Bay of Bengal.

The RAMA and OMNI moorings have enhanced understanding of air-sea interaction in the Bay of Bengal, and we note some of the findings here. The northern Bay of Bengal SST is mainly determined by net heat flux and diffusive mixing, especially during the southwest monsoon season, with a fast response to solar heating (Agarwal et al., 2007). A warming of 1.5°C with peaks that are associated with ISO signatures occurred during August–September 2014 as observed by the RAMA mooring at 15°N, as shown in Figure 5c. The thickness of the ocean surface mixed layer in the northern bay reduced considerably in the past as soon as freshwaters discharged from major rivers like Ganges-Brahmaputra were advected into the open bay, with a time delay of 60 days after the rainfall in the river catchment area (Rao et al., 2011). The warm SST in the north can lead to a large meridional gradient in SST, which plays a major role in the active and break phase of the monsoon (Shankar et al., 2007). The intense warming of the northern bay, with fast response to net heat flux during the southwest monsoon season, was very well observed during 2014, but the warming was not so intense during 2015, even though the surface net heat flux forcing remained the same. Understanding the spatial pattern of the response of SST to surface forcing requires consideration of subsurface processes like vertical

turbulent mixing, and analysis of data from the WHOI mooring, with its high-frequency sampling of subsurface parameters, should yield new insights soon. ◙

REFERENCES

Agarwal, N., R. Sharma, S. Basu, A. Parekh, A. Sarkar, and V.K. Agarwal. 2007. Bay of Bengal summer monsoon 10–20 day variability in sea surface temperature using model and observations. *Geophysical. Research Letters* 34, L06602, http://dx.doi.org/10.1029/2007GL029296.

Bhat, G.S. 2002. Near-surface variations and surface fluxes over the northern Bay of Bengal during the 1999 Indian summer monsoon. *Journal of Geophysical Research* 107(D17), 4336, http://dx.doi.org/10.1029/2001JD000382.

Bigorre, S.P., R.A. Weller, J.B. Edson, and J.D. Ware. 2013. A surface mooring for air–sea interaction research in the Gulf Stream: Part II. Analysis of the observations and their accuracies. *Journal of Atmospheric and Oceanic Technology* 30:450–469, http://dx.doi.org/10.1175/JTECH-D-12-00078.1.

Brunke, M.A., Z. Wang, X. Zeng, M. Bosilovich, and C.-L. Shie. 2011. An assessment of the uncertainties in ocean surface turbulent fluxes in 11 reanalysis, satellite-derived, and combined global datasets. *Journal of Climate* 24:5,469–5,493, http://dx.doi.org/10.1175/2011JCLI4223.1.

Colbo, K., and R.A. Weller. 2009. Accuracy of the IMET sensor package in the subtropics. *Journal of Atmospheric and Oceanic Technology* 26(9):1,867–1,890, http://dx.doi.org/10.1175/2009JTECHO667.1.

Decker, M., M.A. Brunke, Z. Wang, K. Sakaguchi, X. Zeng, and M.G. Bosilovich. 2012. Evaluation of the reanalysis products from GSFC, NCEP, and ECMWF using flux tower observations. *Journal of Climate* 25:1,916–1,944, http://dx.doi.org/10.1175/JCLI-D-11-00004.1.

European Centre for Medium-Range Weather Forecasts. 2012. ERA-Interim Project, Single Parameter 6-Hourly Surface Analysis and Surface Forecast Time Series (updated monthly). Research Data Archive at the National Center for Atmospheric Research, Computational and Information Systems Laboratory, http://dx.doi.org/10.5065/D64747WN.

Fairall, C.W., E.F. Bradley, J.E. Hare, A.A. Grachev, and J.B. Edson. 2003. Bulk paramterization of air-sea fluxes: Updates and verification for the COARE algorithm. *Journal of Climate* 16:571–591, http://dx.doi.org/10.1175/1520-0442(2003)016<0571:BPOASF>2.0.CO;2.

Global Modeling and Assimilation Office. 2008. MERRA, version 5.2.0. Goddard Space Flight Center Distributed Active Archive Center, Greenbelt, MD, USA, http://dx.doi.org/10.5067/4EQ54AKI405R.

Global Modeling and Assimilation Office. 2015. MERRA-2, version 5.12.4. Goddard Space Flight Center Distributed Active Archive Center, Greenbelt, MD, USA, http://dx.doi.org/10.5067/HOVVAD8F6MX5.

Hosom, D.S., R.A. Weller, R.E. Payne, and K.E. Prada. 1995. The IMET (improved meteorology) ship and buoy systems. *Journal of Atmospheric and Oceanic Technology* 12:527–540, http://dx.doi.org/10.1175/1520-0426(1995)012<0527:TIMSAB>2.0.CO;2.

Kalnay, E., M. Kanamitsu, R. Kistler, W. Collins, D. Deaven, L. Gandin, M. Iredell, S. Saha, G. White, J. Woollen, and others. 1996. The NCEP/NCAR 40-Year Reanalysis Project. *Bulletin of the American Meteorological Society* 77:437–471, http://dx.doi.org/10.1175/1520-0477(1996)077<0437:TNYRP>2.0.CO;2.

Kumar, M.R. Ramesh, and T.G. Prasad. 1997. Annual and interannual variation of precipitation over the tropical Indian Ocean. *Journal of Geophysical Research* 108(C8):18,519–18,527, http://dx.doi.org/10.1029/97JC00979.

Lucas, A.J., E.L. Shroyer, H.W. Wijesekera, H.J.S. Fernando, E. D'Asaro, M. Ravichandran, S.U.P. Jinadasa, J.A. MacKinnon, J.D. Nash, R. Sharma, and others. 2014. Mixing to monsoons: Air-sea interactions in the Bay of Bengal. *Eos, Transactions American Geophysical Union* 95(30):269, http://dx.doi.org/10.1002/2014EO300001.

McPhaden, M.J., G. Meyers, K. Ando, Y. Masumoto, V.S.N. Murty, M. Ravichandran, F. Syamsudin, J. Vialard, L. Yu, and W. Yu. 2009. RAMA: The Research Moored Array for African-Asian-Australian Monsoon Analysis and Prediction. *Bulletin of the American Meteorological Society* 90:459–480, http://dx.doi.org/10.1175/2008BAMS2608.1.

Paulson, C.A., and J.J. Simpson. 1977. Irradiance measurements in the upper ocean. *Journal of Physical Oceanography* 7:952–956, http://dx.doi.org/10.1175/1520-0485(1977)007<0952:IMITUO>2.0.CO;2.

Prasad, T.G. 2004. A comparison of mixed-layer dynamics between the Arabian Sea and Bay of Bengal: One-dimensional model results. *Journal of Geophysical Research* 109, C03035, http://dx.doi.org/10.1029/2003JC002000.

Price, J.F., R.A. Weller, and R. Pinkel. 1986. Diurnal cycling: Observations and models of upper ocean response to diurnal heating, cooling, and wind mixing. *Journal of Geophysical Research* 91(C7):8,411–8,427, http://dx.doi.org/10.1029/JC091iC07p08411.

Rao, S.A., S.K. Saha, S. Pokhrel, D. Sundar, A.R. Dhakate, S. Mahapatra, S. Ali, H.S. Chaudhari, P. Shreeram, S. Vasimalla, and others. 2011. Modulation of SST, SSS over northern Bay of Bengal on ISO time scale. *Journal of Geophysical Research* 116, C09026, http://dx.doi.org/10.1029/2010JC006804.

Sengupta, D., G.N. Bharath Raj, and S.S.C. Shenoi. 2006. Surface freshwater from Bay of Bengal runoff and Indonesian Throughflow in the tropical Indian Ocean. *Geophysical Research Letters* 33, L22609, http://dx.doi.org/10.1029/2006GL027573.

Shankar, D., S.R. Shetye, and P.V. Joseph. 2007. Link between convection and meridional gradient of sea surface temperature in the Bay of Bengal. *Journal of Earth System Science* 116(5):385–406, http://dx.doi.org/10.1007/s12040-007-0038-y.

Shenoi, S.S., C.D. Shankar, and S.R. Shetye. 2002. Differences in heat budgets of the near-surface Arabian Sea and Bay of Bengal: Implications for the summer monsoon. *Journal of Geophysical Research* 107(C6), http://dx.doi.org/10.1029/2000JC000679.

Venkatesan, R., V.R. Shamji, G. Latha, S. Mathew, R.R. Rao, A. Muthiah, and M.A. Atmanand. 2013. In situ ocean subsurface time series from OMNI buoy network in the Bay of Bengal. *Current Science* 104(9):1,166–1,177, http://www.currentscience.ac.in/Volumes/104/09/1166.pdf.

Vinayachandran, P.N., V.S.N. Murty, and V. Ramesh Babu. 2002. Observations of barrier layer formation in the Bay of Bengal during summer monsoon. *Journal of Geophysical Research* 107(C12), 8018, http://dx.doi.org/10.1029/2001JC000831.

Weller, R.A., A.S. Fischer, D. Rudnick, C. Eriksen, T. Dickey, J. Marra, C. Fox, and R. Leben. 2002. Moored observations of upper-ocean response to the monsoons in the Arabian Sea during 1994–1995. *Deep Sea Research Part II* 49:2,195–2,230, http://dx.doi.org/10.1016/s0967-0645(02)00035-8.

Weller, R.A., S.P. Bigorre, J. Lord, J.D. Ware, and J.B. Edson. 2012. A surface mooring for air-sea interaction research in the Gulf Stream: Part 1. Mooring design and instrumentation. *Journal of Atmospheric and Oceanic Technology* 29:1,363–1,376, http://dx.doi.org/10.1175/JTECH-D-12-00060.1.

Wijesekera, H.W., E. Shroyer, A. Tandon, M. Ravichandran, D. Sengupta, P. Jinadas, H.J.S. Fernando, N. Agrawal, K. Arulanathan, G.S. Bhat, and others. In press. ASIRI: An Ocean-Atmosphere Initiative for Bay of Bengal. *Bulletin of the American Meteorological Society*, http://dx.doi.org/10.1175/BAMS-D-14-00197.1.

AUTHORS

Robert A. Weller (rweller@whoi.edu) is Senior Scientist and **J. Thomas Farrar** is Associate Scientist, Woods Hole Oceanographic Institution, Woods Hole, MA, USA. **Jared Buckley** is a graduate student at the University of Massachusetts Dartmouth, North Dartmouth, MA, USA. **Simi Mathew** is Scientist and **R. Venkatesan** is Group Head, Ocean Observations, at the National Institute of Ocean Technology, Chennai, India. **J. Sree Lekha** and **Dipanjan Chaudhuri** are graduate students at the Centre for Atmospheric and Oceanic Sciences, Indian Institute of Science, Bangalore, India. **N. Suresh Kumar** is Scientist and **B. Praveen Kumar** is Scientist, Indian National Centre for Ocean Information Services, Hyderabad, India.